



Atomic resolution elemental mapping using energy-filtered imaging scanning transmission electron microscopy with chromatic aberration correction



F.F. Krause^a, A. Rosenauer^a, J. Barthel^{b,c}, J. Mayer^{b,c}, K. Urban^c, R.E. Dunin-Borkowski^c, H.G. Brown^d, B.D. Forbes^d, L.J. Allen^{d,*}

^aInstitute for Solid State Physics and Center of Excellence for Materials and Processes, Bremen University, Otto-Hahn-Allee 1, 28359 Bremen, Germany

^bCentral Facility for Electron Microscopy, RWTH Aachen University, D-52074 Aachen, Germany

^cErnst Ruska-Centre for Microscopy and Spectroscopy with Electrons and Peter Grünberg Institute, Jülich Research Centre, 52425 Jülich, Germany

^dSchool of Physics, University of Melbourne, Parkville, Victoria 3010, Australia

ARTICLE INFO

Article history:

Received 22 February 2017

Revised 11 May 2017

Accepted 1 June 2017

Available online 2 June 2017

Keywords:

Atomic resolution imaging

Elemental mapping

Energy-filtered imaging scanning

transmission electron microscopy

ABSTRACT

This paper addresses a novel approach to atomic resolution elemental mapping, demonstrating a method that produces elemental maps with a similar resolution to the established method of electron energy-loss spectroscopy in scanning transmission electron microscopy. Dubbed energy-filtered imaging scanning transmission electron microscopy (EFISTEM) this mode of imaging is, by the quantum mechanical principle of reciprocity, equivalent to tilting the probe in energy-filtered transmission electron microscopy (EFTEM) through a cone and incoherently averaging the results. In this paper we present a proof-of-principle EFISTEM experimental study on strontium titanate. The present approach, made possible by chromatic aberration correction, has the advantage that it provides elemental maps which are immune to spatial incoherence in the electron source, coherent aberrations in the probe-forming lens and probe jitter. The veracity of the experiment is supported by quantum mechanical image simulations, which provide an insight into the image-forming process. Elemental maps obtained in EFTEM suffer from the effect known as preservation of elastic contrast, which, for example, can lead to a given atomic species appearing to be in atomic columns where it is not to be found. EFISTEM very substantially reduces the preservation of elastic contrast and yields images which show stability of contrast with changing thickness. The experimental application is demonstrated in a proof-of-principle study on strontium titanate.

© 2017 Elsevier B.V. All rights reserved.

1. Introduction

The technique of energy-filtered transmission electron microscopy (EFTEM) uses inelastically scattered electrons that have undergone a specific range of energy losses within a specimen to form an image. Selecting energy windows that cover a range of energies above inner-shell edges pertinent to elements present in the sample, it is possible, in principle, to obtain elemental maps locating different atomic species in the specimen. Until recently, obtaining atomic resolution experimental EFTEM images has been difficult due to chromatic aberration and low signal to noise ratios. Chromatic aberration degrades the image formed, as electrons that have lost different amounts of energy within an energy window will be focused in different planes by the imaging lens. This

effect can be reduced by decreasing the width of the energy window used in image formation, however this also leads to a reduction of the signal to noise ratio. Due to these competing effects, the resolution of energy-filtered images has been limited. Recently chromatic aberration correction has been implemented to supplement the now ubiquitous spherical aberration correctors [1]. The FEI Titan 60–300 PICO at the Ernst Ruska-Centre in Jülich is an example of such a system. This allows wide energy windows to be used, improving signal to noise ratios and sub-Ångstrom resolution can be realized [2,3].

However, despite the improved quality of the elemental maps which can be obtained on such an achromatic system, the interpretation of these images is problematic due to the so-called phenomenon of the preservation of coherent elastic contrast [2–5]. As discussed in detail in Ref. [5], for thicker specimens we find situations where the combination of the delocalized nature of ionization transition potentials and the multiple elastic scattering through the specimen produces features in the EFTEM image, for

* Corresponding author.

E-mail address: lja@unimelb.edu.au (L.J. Allen).

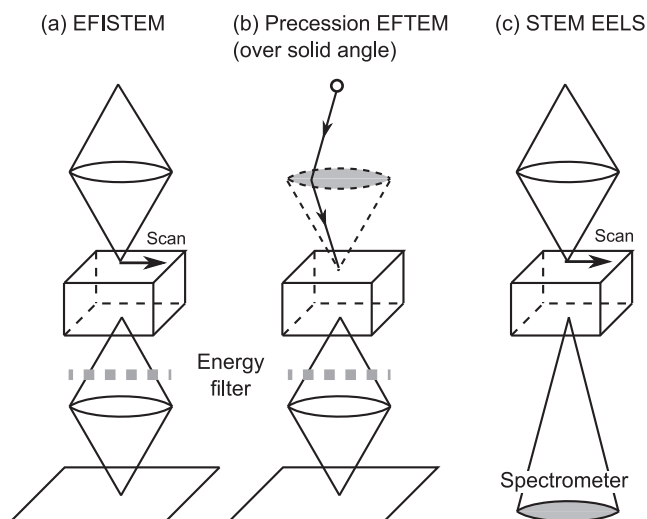


Fig. 1. Schematic showing (a) energy-filtered scanning transmission electron microscopy (EFISTEM), (b) precession energy-filtered transmission electron microscopy (precession EFTEM) and (c) scanning transmission electron microscopy (STEM) using electron energy-loss spectroscopy (EELS).

which plane wave (parallel) illumination is used, that do not allow for reliable interpretation by visual analysis alone. In Ref. [3] it was found that EFTEM images of strontium titanate (STO) down the [001] zone axis based on the titanium $L_{2,3}$ -edge and the oxygen K -edge were not directly interpretable as elemental maps of titanium and oxygen. Due to the delocalized nature of the transition potentials associated with these core-loss edges, a particular column containing the element of interest makes a delocalized contribution to the EFTEM image contrast. In particular intensity is seen around columns as far as 0.3 nm away from the column in which the inelastic scattering event occurred. Localization of elemental information in EFTEM maps for these edges is only possible for very thin specimens (<3 nm).

2. Energy-filtered imaging scanning transmission electron microscopy (EFISTEM)

2.1. Experimental setup and relationship to other imaging modes

The imaging scanning transmission electron microscopy (ISTEM) mode introduced by Rosenauer, Krause et al. [6] could be a way to address the effects of preservation of elastic contrast in EFTEM. ISTEM effectively implements transmission electron microscopy (TEM) imaging with spatially incoherent illumination (filling a cone with angle analogous to that of the probe-forming semi-angle used in the ISTEM experiment). This is implemented by using, for image formation in TEM, a strongly focused probe scanning (sequentially) over the sample area of interest instead of employing parallel (simultaneous) illumination. Since the acquisition time is identical to the total scan time, the resulting image consists of all the incoherently overlapping intensity distributions created by the continuously scanning beam. Incoherent image formation allows increased resolution and is more robust with respect to chromatic aberration than the coherent illumination used in conventional TEM (CTEM) [6,7]. The same strategy is implemented here but now with an energy filter in place, dubbed energy-filtered ISTEM (EFISTEM). The energy-filtered image is built up by incoherently summing the images obtained as a STEM probe is scanned across the specimen. This is shown schematically in Fig. 1(a). This yields the same image that would be obtained if we were to tilt the wave vector of an incident plane wave through a range of angles similar to that defined by the probe-forming aperture in EFIS-

TEM, as shown in Fig. 1(b) [8] and referred to here as precession EFTEM. Tilting the illumination through a range of angles in TEM is an approach discussed in Ref. [9], where it is referred to as hollow-cone illumination TEM. Precession EFTEM would, however, be less convenient to implement experimentally than EFISTEM. In Ref. [8] it was demonstrated using simulations, comparing conventional EFTEM images to EFISTEM images, that for the latter the preservation of elastic contrast is indeed strongly suppressed. By the quantum mechanical principle of reciprocity, it can be shown that the commonly used STEM EELS configuration shown in Fig. 1(c) is approximately equivalent to both the EFISTEM and precession EFTEM cases shown in Fig. 1(a) and (b). STEM EELS suffers from resolution-limiting factors such as spatial incoherence, due to the finite size of the electron source, and scan noise, as discussed in Ref. [8]. Aberrations in the condenser lens can affect the probe but STEM EELS is immune to imaging system aberrations and image spread phenomena. EFISTEM, on the other hand, provides elemental maps which are immune to spatial incoherence in the electron source and probe scan jitter, but is affected by image spread and the modulation transfer function of the camera used. Furthermore, the maps are also insensitive to coherent aberrations in the probe-forming lens but are affected by aberrations in the post-specimen image-forming lens. The aberrations in the image-forming lens are negligible in a system with spherical and chromatic aberration correction, such as that used here, but may be problematic in non-corrected systems.

2.2. Potential resolution of EFISTEM relative to STEM EELS

The resolution of EFISTEM images is therefore determined by the limitations of the microscope used (in this case the PICO instrument) for the energy window selected. Depending on the chosen magnification, the modulation transfer function of the camera may lead to a significant contrast reduction. Due to the very high magnification applied in the experiment to be described in the next paragraph, that is not the case here. The essential limitation is hence due to an image spread [1] characterized by a root-mean-square amplitude of 16 pm. While scan noise and source size, which limit STEM EELS, typically amount to a broadening of more than 80 pm (HWHM) [10,11], the image spread of 16 pm corresponds to a broadening of only 19 pm (HWHM). This shows the potential of EFISTEM as a complementary method to yield increased spatial resolution compared to STEM EELS for specific experimental conditions and applications. This is at the expense of the acquired spectral information, as STEM EELS yields complete spectra for each scan point, while EFISTEM will result in one specific elemental map.

3. Experiment

We have taken both ISTEM and EFISTEM images of a specimen of STO, approximately 15 nm thick, down the [001] zone axis using the FEI Titan 60–300 PICO at the ER-C Jülich [12], currently one of only a handful of microscopes worldwide with chromatic aberration correction. The STO specimen was prepared using focused ion beam and low-energy Ar-ion milling to obtain a lamella with an edge thickness between 10 and 20 nm. The microscope was operated at 200 kV, with a probe forming aperture of 20 mrad, which was chosen to get good contrast in the ISTEM images. The coherent aberrations were corrected up to 22 mrad following the $\pi/4$ criterion [13]. No hard objective aperture was used on the image forming lens but the contrast transfer function is limited by an effective aperture which is caused by mechanical vibrations, lens instabilities and, for the PICO instrument, especially by thermal magnetic field noise [14], which which act together as an effective

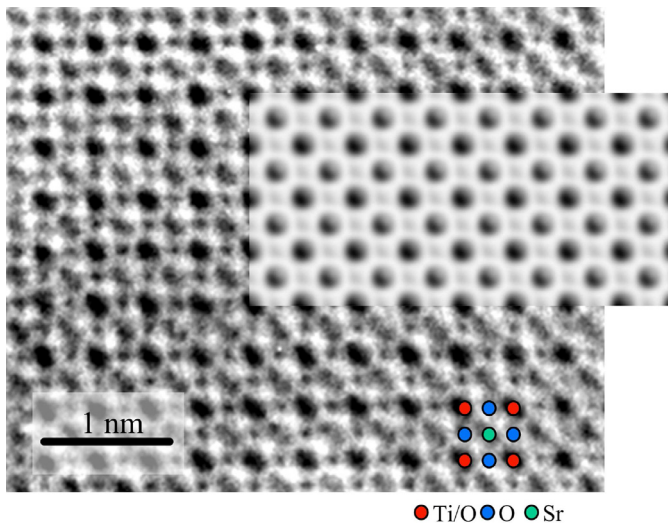


Fig. 2. Experimental imaging scanning transmission electron microscopy (ISTEM) image of strontium titanate taken down the [001] zone axis at 200 kV with a probe-forming semi-convergence angle of 20 mrad. The simulation which is overlaid used these parameters and assumed that the probe was tilted by 3 mrad along [110] and that the imaging lens was underfocused by 12.5 nm and had an effective aperture of 55 mrad. A Gaussian blur with a HWHM of 0.035 nm has been applied to the simulation.

image spread [15]. The effective aperture was characterized in simulations using a semi-angle of 55 mrad (at 200 keV corresponding to a maximum resolution of 25 pm in real space) [1].

The ISTEM image was acquired by setting the energy filter to have a slit width of 25 eV around the zero-loss peak and is shown in Fig. 2. A simulation is overlaid, in which, to take into account specimen tilt in the experiment, we assumed a tilt of 3 mrad in the [110] direction. We also assumed that the image forming lens was underfocused by 12.5 nm and had an effective aperture of 55 mrad. Agreement between the simulation and experiment was obtained by further assuming a specimen thickness of 15 nm and by applying a Gaussian blur with a HWHM of 0.035 nm to the raw simulated image to take into account the limitations discussed at the end of the last paragraph as well as specimen instabilities and contamination. The pure oxygen columns are readily visible in the ISTEM image, as are the titanium/oxygen and strontium columns.

For this same specimen we now record three separate images with a 25 eV energy window centered at 491 eV, 514 eV and 547 eV using the Gatan Quantum energy filter of the PICO microscope. The area and pixel size of the scan were chosen to be similar to those of the camera. The energy loss selection was achieved by elevating the acceleration voltage [2]. The energies of the first two images are pre-edge and the final image is post the oxygen *K*-edge (532 eV). To obtain an elemental map, the three images were registered, and the average of the two pre-edge images was subtracted from the post edge image after multiplication by a factor that was chosen in such a way that the minimum intensity in the difference was close to zero. This is based on the hypothesis that the signal intensity contribution of the *K*-edge is close to zero in some areas of the image. This unorthodox method for the three-window evaluation was used because the conventional technique of fitting exponential decays to the pre-edge images failed, due to noise and specimen-contamination during the acquisition. The reason for these obstacles is the fact that the voltage setting and the alignment of scan area and camera had to be done manually for each of the three EFISTEM images as there are no automated routines yet, as exist for conventional EFTEM. Thus a large fraction of the dose is not used for the actual image acquisition. This could be improved in the future by an automated routine. This approach

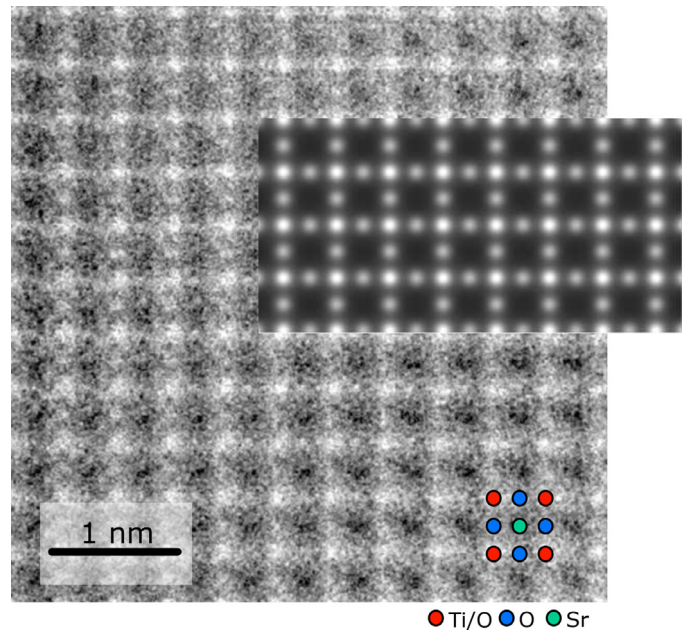


Fig. 3. Experimental energy-filtered scanning transmission electron microscopy (EFISTEM) oxygen map of strontium titanate taken down the [001] zone axis at 200 kV with a probe forming semi-convergence angle of 20 mrad. The simulation which is overlaid used these parameters and also assumed that the probe was focused on the entrance surface of the specimen and that the imaging lens had an effective aperture of 55 mrad. The same Gaussian blur that was applied to the simulated ISTEM image in Fig. 2 was also used in this case.

gives the energy-filtered map shown in Fig. 3, which, for improvement of the signal-to-noise ratio, was formed by shifting the image in multiples of the lattice constant left and right and up and down by three unit cells and then averaging over these images under the assumption that the specimen does not change over this area. There is now a minimum signal (dark contrast) at the position of the (pure) Sr columns. There is a strong signal from O on the Ti/O columns and a more diffuse signal is evident at the sites of the pure O columns. This clearly demonstrates that EFISTEM allows one to acquire elemental maps. A simulation of the EFISTEM image for the given experimental conditions and assuming a specimen of thickness 15 nm (overlaid in Fig. 3) firstly confirms that, in this case, the oxygen signal is a minimum on the Sr columns and this is consistent with the background subtraction procedure used for this particular set of experimental conditions. We also see that one should expect a reduced signal on the pure O columns, a result which also occurs in the reciprocal STEM EELS geometry and which has been discussed in detail in Ref. [16]. The signal on the pure O columns is compromised by a low signal to noise ratio in the experimental image. The contrast was optimized in the experiment and simulation clearly suggests that this was achieved around zero defocus, unlike the substantial underfocus for the separately acquired ISTEM image in Fig. 2. The same Gaussian blur inferred from the ISTEM image in Fig. 2 (HWHM 0.035 nm) has been applied here. That the defocus of the imaging lens can be decisively deduced is shown by the simulated EFISTEM through-focal series in Fig. 4(a) (no Gaussian blur applied). This series is plotted on a common gray scale and therefore is an indication of how contrast changes as the defocus of the imaging lens changes. The contrast was optimized in the experiment and simulation clearly suggests that this was around zero defocus. A similar focal series calculated for EFTEM in Fig. 4(b) shows that defocus value at which the best contrast occurs is not as well defined in that case.

The thickness of the specimen was estimated to be around 15 nm by comparing high-angle annular dark-field STEM images

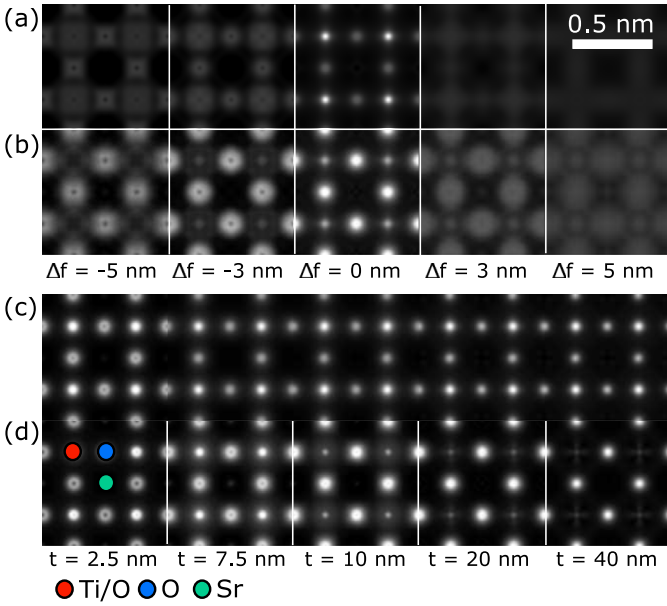


Fig. 4. (a) The EFISTEM simulation in Fig. 3 is compared with defocus values around zero defocus of the image forming lens (underfocus values are negative). The contrast in this through focal series is on a common contrast scale to best represent what would be seen in the microscope. The best contrast is clearly obtained at zero defocus. In (b) we have a similar defocus series for EFTEM under the same imaging conditions. (c) The EFISTEM simulation in Fig. 3 can be compared with these EFISTEM images for a range of thickness values (all at zero defocus). The image for each thickness is on its own contrast scale. (d) EFTEM images for the same conditions as in (c) but for EFTEM.

to simulations [17–19]. This thickness was used in the simulation of the ISTEM image in Fig. 2 and by varying the defocus agreement between experiment and theory could be obtained. The EFISTEM simulations for a wide range of thicknesses around that value are shown in Fig. 4(c). What is remarkable is the stability in contrast of the EFISTEM images as the thickness varies. This is not the case for equivalent EFTEM images, as shown in Fig. 4(d).

4. Theory and simulation

We calculated the ISTEM, EFISTEM and EFTEM images using the quantum excitation of phonons (QEP) model [20]. In the context of the QEP model, the key equation used to calculate the intensity in the recording plane for the EFISTEM (for each probe position) and EFTEM simulations is given by [2]

$$I(\mathbf{r}) = \int \sum_{\alpha,n} |T(\mathbf{r}) \otimes \phi_{\alpha,n}(\mathbf{r}, t, \boldsymbol{\tau})|^2 |a_0(\boldsymbol{\tau})|^2 d\boldsymbol{\tau}, \quad (1)$$

where $T(\mathbf{r})$, with \mathbf{r} perpendicular to the optical axis, is the transfer function of the imaging lens and is convolved with the auxiliary functions $\phi_{\alpha,n}(\mathbf{r}, t, \boldsymbol{\tau})$ that represent an electron at the exit surface of a specimen with thickness t after the ionization of atom α to leave the system in a final state n . Final states that are consistent with the settings of the energy filter are taken into account. The integration is a quantum mechanical average over nuclear coordinates, where $|a_0(\boldsymbol{\tau})|^2$, the modulus squared of the wave function describing the nuclear subsystem for the set of nuclear coordinates $\boldsymbol{\tau}$, acts as a probability distribution and takes into account the crystal being in a superposition of phonon states. If the atom labeled by α is at a depth z in the specimen, then the auxiliary function at the exit surface, $\phi_{\alpha,n}(\mathbf{r}, t, \boldsymbol{\tau})$ in Eq. (1), is obtained after channeling the auxiliary function generated at z , immediately after ionization, through the distance $t - z$ to the exit surface. For EFISTEM simulations, Eq. (1) is calculated for different positions of

the focused probe and the resulting intensities are then summed incoherently. The generation of the auxiliary function at z due to an ionization event is given by [20,21]

$$\phi_{\alpha,n}(\mathbf{r}, z, \boldsymbol{\tau}) = \frac{m}{2\pi i \hbar^2 k_n} H_{\alpha,n0}(\mathbf{r}, \boldsymbol{\tau}) \phi_0(\mathbf{r}, z, \boldsymbol{\tau}). \quad (2)$$

Here m is the (relativistically corrected) electron mass and k_n is the wave number of the electron after the inelastic scattering event (also relativistically corrected). The modulus squared of the transition potential $H_{\alpha,n0}(\mathbf{r}, \boldsymbol{\tau})$, for an excitation of atom α from the initial (bound) state denoted by 0 to the continuum state n after ionization, gives the probability of that transition occurring. The dependence on $\boldsymbol{\tau}$ indicates that the potential moves with the atom for each new configuration considered. The function $\phi_0(\mathbf{r}, z, \boldsymbol{\tau})$ associated with the electron prior to ionization is obtained by channeling the incident wave from the entrance surface for the configuration of atoms specified by $\boldsymbol{\tau}$. We use an angular momentum basis to represent the transition potentials, the actual calculation of which are described in detail elsewhere [22]. It is the delocalization of these potentials that determines the degree of preservation of elastic contrast, in particular in EFTEM.

5. Summary and conclusions

We have demonstrated the acquisition of elemental maps using an incoherent approach to EFTEM, namely energy-filtered imaging STEM (EFISTEM) that substantially reduces the effects of the preservation of elastic contrast and provides more directly interpretable images than those obtained in conventional EFTEM. This more incoherent approach is equivalent to tilting the probe through all angles inside a cone and incoherently adding the results but has the advantage that it is easier to implement. Additional merits of this approach are that it is immune to spatial incoherence in the electron source, coherent aberrations in the probe forming lens and also to probe noise. Furthermore the contrast in EFISTEM maps was found to be remarkably stable when varying specimen thickness. A fundamental understanding of the imaging physics, based on calculations from first principles, has also been presented.

Acknowledgements

This research was supported by the Deutsche Forschungsgemeinschaft (Contract No. RO2057/4-2) and by the Discovery Projects funding scheme of the Australian Research Council (Project No. DP110102228).

References

- [1] M. Haider, P. Hartel, H. Müller, S. Uhlemann, J. Zach, Information transfer in a tem corrected for spherical and chromatic aberration, *Microsc. Microanal.* 16 (04) (2010) 393–408.
- [2] K.W. Urban, J. Mayer, J.R. Jinschek, M.J. Neish, N.R. Lugg, L.J. Allen, Achromatic elemental mapping beyond the nanoscale in the transmission electron microscope, *Phys. Rev. Lett.* 110 (2013) 185507.
- [3] B.D. Forbes, L. Houben, J. Mayer, R.E. Dunin-Borkowski, L.J. Allen, Elemental mapping in achromatic atomic-resolution energy-filtered transmission electron microscopy, *Ultramicroscopy* 147 (2014) 98–105.
- [4] P. Stallknecht, H. Kohl, Computation and interpretation of contrast in crystal lattice images formed by inelastically scattered electrons in a transmission electron microscope, *Ultramicroscopy* 66 (3) (1996) 261–275.
- [5] N.R. Lugg, B. Freitag, S.D. Findlay, L.J. Allen, Energy-filtered transmission electron microscopy based on inner-shell ionization, *Ultramicroscopy* 110 (2010) 981–990.
- [6] A. Rosenauer, F.F. Krause, K. Müller, M. Schowalter, T. Mehrtens, Conventional transmission electron microscopy imaging beyond the diffraction and information limits, *Phys. Rev. Lett.* 113 (9) (2014) 096101.
- [7] K. van den Bos, F. Krause, A. Béché, J. Verbeeck, A. Rosenauer, S. Van Aert, Locating light and heavy atomic column positions with picometer precision using ISTEM, *Ultramicroscopy* 172 (2017) 75–81.
- [8] H.G. Brown, A.J. D'Alfonso, B.D. Forbes, L.J. Allen, Addressing preservation of elastic contrast in energy-filtered transmission electron microscopy, *Ultramicroscopy* 160 (2016) 90–97.

- [9] C. Dinges, H. Kohl, H. Rose, High-resolution imaging of crystalline objects by hollow-cone illumination, *Ultramicroscopy* 55 (1) (1994) 91–100, doi:[10.1016/0304-3991\(94\)90083-3](https://doi.org/10.1016/0304-3991(94)90083-3).
- [10] J. Verbeeck, A. Beche, W. Van den Broek, A holographic method to measure the source size broadening in STEM, *Ultramicroscopy* 120 (2012) 35–40, doi:[10.1016/j.ultramic.2012.05.007](https://doi.org/10.1016/j.ultramic.2012.05.007).
- [11] L. Jones, P.D. Nellist, Identifying and correcting scan noise and drift in the scanning transmission electron microscope, *Microsc. Microanal.* 19 (2013) 1050–1060, doi:[10.1017/S1431927613001402](https://doi.org/10.1017/S1431927613001402).
- [12] J. Barthel, L. Houben, K. Tillmann, FEI Titan G3 50-300 PICO, *J. Large Scale Res. Facilities* 1 (2015) 34.
- [13] S. Uhlemann, M. Haider, Residual wave aberrations in the first spherical aberration corrected transmission electron microscope, *Ultramicroscopy* 72 (3) (1998) 109–119.
- [14] S. Uhlemann, H. Müller, P. Hartel, J. Zach, M. Haider, Thermal magnetic field noise limits resolution in transmission electron microscopy, *Phys. Rev. Lett.* 111 (4) (2013) 046101.
- [15] C. Jia, S. Mi, J. Barthel, D. Wang, R. Dunin-Borkowski, K. Urban, A. Thust, Determination of the 3D shape of a nanoscale crystal with atomic resolution from a single image, *Nat. Mater.* 13 (11) (2014) 1044–1049.
- [16] B.D. Forbes, A.J. D'Alfonso, R.E.A. Williams, R. Srinivasan, H.L. Fraser, D.W. McComb, B. Freitag, D.O. Klenov, L.J. Allen, Contribution of thermally scattered electrons to atomic resolution elemental maps, *Phys. Rev. B* 86 (2012) 024108, doi:[10.1103/PhysRevB.86.024108](https://doi.org/10.1103/PhysRevB.86.024108).
- [17] A. Rosenauer, T. Mehrrens, K. Müller, K. Gries, M. Schowalter, P.V. Satyam, S. Bley, C. Tessarek, D. Hommel, K. Sebald, M. Seyfried, J. Gutowski, A. Avramescu, K. Engl, S. Lutgen, Composition mapping in InGaN by scanning transmission electron microscopy, *Ultramicroscopy* 111 (8) (2011) 1316–1327, doi:[10.1016/j.ultramic.2011.04.009](https://doi.org/10.1016/j.ultramic.2011.04.009).
- [18] T. Grieb, K. Müller, R. Fritz, M. Schowalter, N. Neugebohrn, N. Knaub, K. Volz, A. Rosenauer, Determination of the chemical composition of GaNAs using STEM HAADF imaging and STEM strain state analysis, *Ultramicroscopy* 117 (2012) 15–23, doi:[10.1016/j.ultramic.2012.03.014](https://doi.org/10.1016/j.ultramic.2012.03.014).
- [19] M. Tewes, F.F. Krause, K. Müller, P. Potapov, M. Schowalter, T. Mehrrens, A. Rosenauer, Quantitative composition evaluation from HAADF-STEM in GeSi/Si heterostructures, *J. Phys. Conf. Ser.* 471 (1) (2013) 012011, doi:[10.1088/1742-6596/471/1/012011](https://doi.org/10.1088/1742-6596/471/1/012011).
- [20] B.D. Forbes, A.V. Martin, S.D. Findlay, A.J. D'Alfonso, L.J. Allen, Quantum mechanical model for phonon excitation in electron diffraction and imaging using a Born-Oppenheimer approximation, *Phys. Rev. B* 82 (10) (2010) 104103, doi:[10.1103/PhysRevB.82.104103](https://doi.org/10.1103/PhysRevB.82.104103).
- [21] W. Coene, D. Van Dyck, Inelastic scattering of high-energy electrons in real space, *Ultramicroscopy* 33 (1990) 261–267.
- [22] S.D. Findlay, M.P. Oxley, L.J. Allen, Modeling atomic-resolution scanning transmission electron microscopy images, *Microsc. Microanal.* 14 (01) (2008) 48–59, doi:[10.1017/S1431927608080112](https://doi.org/10.1017/S1431927608080112).